JOURNAL OF GEOPHYSICAL RESEARCH, VOL. 118, 1–11, doi:10.1029/2012JA017972, 2013

Nature of axial tail instability and bubble-blob formation in near-Earth plasma sheet

P. Zhu,[1] J. Raeder,[2] C. C. Hegna,[1] and C. R. Sovinec[1]

Received 23 May 2012; revised 22 October 2012; accepted 22 November 2012.

[1] Previous global magnetohydrodynamic (MHD) simulations of substorm events have identified the dynamic presence of an axial tail instability that is uniform in the dawn-dusk direction in the near-Earth plasma sheet. The axial tail instability is found to be a major cause of the initial growing MHD force imbalance on closed field lines prior to the subsequent magnetic reconnection and substorm expansion onset processes. In this work, energy principle analysis indicates that a two-dimensional thin current sheet configuration in the magnetotail is typically stable to the axial mode within the framework of ideal MHD model. However, linear resistive MHD calculations find axial tail instabilities on closed field lines in the generalized Harris sheet configurations. The properties of these instabilities are similar to the axial tail modes observed in the global MHD simulations. The axial tail mode is unstable in regimes of low Lundquist number and regions with small normal component of magnetic field. Such resistive axial tail instability would by many researchers be considered as tearing instability in a two-dimensional tail configuration. Unlike the conventional tearing mode of Harris sheet, the linear axial tail instability does not involve any reconnection process. Instead, the nature of the mode is dominantly a slippage process among neighboring flux tubes as facilitated by resistive dissipation. A natural consequence of the axial tail instability is shown to be the formation of bubble-blob pairs in the pressure and entropy profiles in the near-Earth plasma sheet.

Citation: Zhu, P., J. Raeder, C. C. Hegna, and C. R. Sovinec (2013), Nature of axial tail instability and bubble-blob formation in near-Earth plasma sheet, *J. Geophys. Res.*, *118*, doi:10.1029/2012JA017972.

1. Introduction

[2] Recent global MHD simulations indicate that substorm onsets are often preceded by a growing MHD force imbalance in a near-tail region where the northward component of magnetic field normal to the current sheet is finite [*Siscoe et al.*, 2009]. The X-line structure in the magnetic field, a characteristic feature of two-dimensional (2D) magnetic reconnection, does not form initially. However, X-line formation does occur just before the expansion onset. Further examination of the global simulations using the OpenGGCM (Open Geospace General Circulation Model) code shows the growth of an MHD mode with $k_y = 0$ on closed field lines in the near-Earth tail prior to reconnection events that lead to onset [*Raeder et al.*, 2010]. Here the coordinate system is chosen so that the x axis is in Sun-Earth (tailward) direction, the y axis in dusk-dawn direction, and the z axis in south-north direction. k_y is the azimuthal wavenumber in the y direction. This mode is uniform in the dusk-dawn direction and is therefore referred to as an axial tail mode or instability. The axial tail mode is ideal-like in the sense that the field line topology is intact in contrast to instabilities involving 2D reconnection. However, this instability shares some similarities with the resistive tearing mode in terms of mode growth rate and structure. The nonlinear development of the axial mode is found to initiate ballooning instability by setting up a favorable plasma sheet configuration. This occurs before the formation of an X-line and the onset of reconnection [*Zhu et al.*, 2009]. Recently, it was found in RCM (Rice Convection Model) and OpenGGCM simulations that the formation of an entropy bubble-blob pair in the near-Earth magnetotail can accelerate the thinning of the current sheet and provide a feedback mechanism for the formation of the near-Earth neutral line and the onset of reconnection [*Yang et al.*, 2011; *Hu et al.*, 2011]. The dynamic development of the bubble-blob pair is closely related to the growth of the axial mode in OpenGGCM simulations.

[3] A number of questions arise about the nature of the axial mode identified in the global MHD simulations. Does the axial mode develop from a linear eigenmode of an equilibrium configuration or merely a convection process driven by the electric field present at the magnetopause? Is the axial mode an ideal or resistive MHD process? Is the MHD process pressure driven or tearing? Is the formation of the bubble-blob pair an integral aspect of the axial mode?

[1]Department of Engineering Physics and Department of Physics, University of Wisconsin-Madison, Madison, Wisconsin, USA.
[2]Space Science Center and Physics Department, University of New Hampshire, Durham, New Hampshire, USA.

Corresponding author: P. Zhu, Department of Engineering Physics and Department of Physics, University of Wisconsin-Madison, 1500 Engineering Drive, Madison, WI 53706, USA. (pzhu @wisc.edu)

0148-0227/13/2012JA017972

To address these questions, we have developed an ideal MHD energy principle analysis and a resistive MHD calculation of the stability of an idealized 2D current sheet configurations that is meant to model the near-Earth magnetotail configuration associated with the axial mode in OpenGGCM simulations. We are particularly interested in understanding the nature of the initial growing MHD force imbalance that itself clearly does not involve reconnection but appears to trigger the subsequent reconnection and onset of substorm expansion in global MHD simulations [*Siscoe et al*., 2009; *Raeder et al*., 2010]. This study is intended to provide an interpretation of the recent group of published work on the axial tail instability and the bubble-blob pair formation within the framework of the MHD model [*Siscoe et al*., 2009; *Raeder et al*., 2010; *Hu et al*., 2011]. Whereas MHD model cannot account for the kinetic mechanisms in the reconnection process, the MHD approach to magnetospheric plasma modeling has been able to account for the major macro spatial and temporal scales associated with substorm onset process [e.g., *Raeder et al*., 2008]. It is a first step towards a full understanding of substorm observations.

[4] Our MHD energy principle analysis indicates that the axial mode ($k_y = 0$) in 2D tail configuration is stable at lowest order in B_z/B_x with the ideal MHD constraint (i.e., the "frozen-in-flux" condition). Here B_x and B_z are components of tail magnetic field in x and z directions, respectively. Resistive MHD calculations using the NIMROD (Non-Ideal Magnetohydrodynamics with Rotation - Open Discussion) code [*Sovinec et al*., 2004] find linearly growing axial modes on closed field lines in the generalized Harris sheet. These modes are more unstable in low Lundquist number regimes and regions with weak magnetic normal component. The scaling of the linear growth rate and the mode structure show both similarities and differences in comparison to the Harris sheet tearing and resistive interchange modes. The formation of the entropy bubble-blob pair is actually a natural consequence of this axial instability. There are qualitative similarities between the axial instabilities in the generalized Harris sheet and the ones associated with the initial growing MHD force imbalance as found in OpenGGCM simulations. This suggests that the latter can indeed be a spontaneous, internal instability process. The nonlinear development of this instability should provide an intrinsic mechanism for the initiation of a fast and spontaneous formation of the neutral line in near-Earth plasma sheet. One may infer from these findings that even though reconnection process often precedes a substorm onset expansion, the onset trigger process may not start from reconnection out of a 2D current sheet equilibrium. The reconnection process itself can be initiated by the axial tail instability, which is a non-reconnecting, flux-tube slippage process on closed field lines with finite B_z in the near-Earth magnetotail.

[5] The axial tail instability studied here appears to have similar growth and structure to those of the mode previously described as a resistive tearing instability of the 2D magnetotail current sheet. There is a long history of analytical and numerical work on the resistive tearing instability of the 2D magnetotail current sheet with finite B_z in the context of substorm trigger problem [e.g., *Schindler*, 1974; *Galeev and Zelenyi*, 1976; *Birn et al*., 1975; *Birn*, 1980; *Janicke*, 1980; *Hesse and Birn*, 1994; *Harrold et al*., 1995; *Sundaram and Fairfield*, 1997; *Sitnov et al*., 2002]. However, the nature of the linear axial tail instability in our calculations is not strictly "tearing" in the sense that its dynamics does not involve a reconnection process which would change the topology of the magnetic field. In fact, the presence of a normal component of the magnetic field in a 2D current sheet strongly inhibits the linear tearing or reconnecting process, both topologically and dynamically [*Harrold et al*., 1995]. Instead, what takes place when an axial tail mode becomes unstable is a slippage process driven by the free energy released from the pressure gradient along the axial (or tailward) direction, which would not have been possible in the 2D x-z plane with the ideal MHD "frozen-in-flux" condition. As shown in the following calculations, the redistribution of pressure or entropy through the slippage process is part of a feedback mechanism that enables the formation and growth of a linear axial eigenmode in the 2D x-z plane of the magnetotail in the absence of reconnection.

[6] There has also been series of theoretical analyses and numerical simulations that have employed collisionless kinetic models to address the question whether the 2D magnetotail plasma can be unstable to the tearing-like, axial tail mode perturbations. It was first revealed by *Lembége and Pellat* [1982] that the ion tearing mode is stable in 2D current sheets with finite B_z due to the magnetization of electrons. Similar results were obtained later in theory analyses [*Pellat et al*., 1991; *Brittnacher et al*., 1994; *Quest et al*., 1996] and particle-in-cell (PIC) simulations [*Pritchett*, 1994; *Pritchett and Büchner*, 1995]. Those kinetic analyses and PIC simulations assume both isotropy and gyrotropy in equilibrium particle distributions, and they find the ion tearing mode stable in the regime defined by $\lambda \gtrsim \rho_i$ and $k_x\rho_e < 1$. Here λ is the scale of current sheet width, ρ_i the average ion gyroradius in the asymptotic magnetic field $B_0 = B(z = \pm\infty)$, k_x the wavenumber of perturbation in x direction, and ρ_e the electron gyroradius in the normal component B_z. However, when $B_z \to 0$, electrons become less magnetized and those modes with $k_x\rho_e \gtrsim 1$ can indeed have slow growth which eventually lead to the formation of X-line and subsequent fast reconnection, as found in the PIC simulations by *Pritchett and Büchner* [1995]. Recently, 2D PIC simulations have found slowly growing modes on closed field lines in $k_x\rho_e \lesssim 1$ and $k_x\rho_i \gtrsim 1$ regime for a certain type of multi-scale generalized Harris sheets [*Sitnov and Swisdak*, 2011]. Those modes from kinetic simulations seem to share many similar features with the axial tail instability in our calculations, including the formation of a bubble-blob pair and the subsequent appearance of an X-line from the initially closed field line region.

[7] This work, however, is not meant to reconcile the difference in basic assumptions and predictions between the resistive MHD model and the collisionless kinetic model for the ion tearing mode in the magnetotail with finite B_z component, nor is this work meant to be a direct or substantial advance on the theory of the resistive tearing mode in the magnetotail by incorporating relevant kinetic electron physics in MHD model. This work is a follow-up study intended to interpret the presence of the axial tail instability and the associated bubble-blob pair formation recently found in global MHD simulations of a substorm event [*Raeder et al*., 2010; *Hu et al*., 2011]. For that purpose, we have adopted essentially the same resistive MHD model as that used in those global MHD simulations. In spite of the fact

that the magnetotail plasma is nearly collisionless, it is also well known that the magnetotail plasma sheet plasma is almost always turbulent [e.g., *Borovsky and Funsten*, 2003; *Weygand et al*., 2005]. The turbulence in the plasma sheet can produce dissipation and anomalous resistivity, with an effective Lundquist number ranging from the order of tenths to tens for the active, thinned near-Earth plasma sheet [*Cattell*, 1996]. Nonetheless, caution should be exercised when directly applying numerical simulation results to the interpretation of magnetotail observations.

[8] The rest of the paper is organized as follows. We first present in section 2 an ideal MHD energy principle analysis of 2D magnetotail configuration in terms of an axial mode in a thin plasma sheet. We then report NIMROD calculations of linear MHD instability of two types of current sheet configurations constructed from generalized Harris sheet equilibrium in section 3. We summarize and discuss our findings in section 4.

2. Ideal MHD Energy Principle Analysis

[9] The ideal MHD energy principle was originally developed for the stability analysis of magnetically confined plasma in laboratory [*Bernstein et al*., 1958]. *Miura* [2007] later extended the energy principle to the analysis of MHD stability of semi-confined plasma on closed field lines in the magnetotail, where the change of potential energy $\delta W = W_F + \delta W_S$, and the fluid energy δW_F and the surface energy δW_S are given, respectively, by

$$\delta W_F = \frac{1}{2}\int dV\left[|\mathbf{Q}_\perp|^2 + B^2|2\boldsymbol{\kappa}\cdot\boldsymbol{\xi}_\perp + \nabla\cdot\boldsymbol{\xi}_\perp|^2 + \gamma p|\nabla\cdot\boldsymbol{\xi}|^2 - J_\parallel\left(\boldsymbol{\xi}_\perp^*\times\mathbf{b}\right)\cdot\mathbf{Q}_\perp - 2\left(\boldsymbol{\kappa}\cdot\boldsymbol{\xi}_\perp^*\right)\left(\boldsymbol{\xi}_\perp\cdot\nabla p\right)\right] \quad (1)$$

$$\delta W_S = \frac{1}{2}\int d\mathbf{S}\cdot\left[\boldsymbol{\xi}^*(-\gamma p)\nabla\cdot\boldsymbol{\xi} + \boldsymbol{\xi}_\perp^*(\mathbf{B}\cdot\mathbf{Q} - \boldsymbol{\xi}_\perp\cdot\nabla p) - \mathbf{B}(\boldsymbol{\xi}^*\cdot\mathbf{Q})\right] \quad (2)$$

Here the equilibrium fields include magnetic field $\mathbf{B}$, field-line-aligned current $J_\parallel$, and pressure p (all subscripts "0" are omitted from equilibrium fields for simplicity). In addition, $B = |\mathbf{B}|$, $\mathbf{b} = \mathbf{B}/B$, and magnetic curvature $\boldsymbol{\kappa} = \mathbf{b}\cdot\nabla\mathbf{b}$. The plasma displacement is denoted as $\boldsymbol{\xi}$, and the perturbed magnetic field $\mathbf{Q} = \nabla\times(\boldsymbol{\xi}\times\mathbf{B})$. The specific heat ratio $\gamma = 5/3$. The superscript "*" denotes a complex conjugate, and the subscript "$\perp$" ("$\parallel$") denotes the perpendicular (parallel) component relative to the equilibrium magnetic field direction. The integrals $\int dV$ and $\int d\mathbf{S}$ are over the spatial volume and surface of the physical domain, respectively. The meanings of other symbols are conventional. The surface contribution δW_S vanishes for certain boundary conditions at the ionosphere, such as $\nabla\cdot\boldsymbol{\xi} = 0$ and $\boldsymbol{\xi}_\perp = 0$, or $\xi_\parallel = 0$ and $\boldsymbol{\xi}_\perp = 0$. We consider a static 2D ideal MHD equilibrium $\mathbf{B} = -\nabla\Psi(x,z)\times\mathbf{e}_y$ for the magnetotail and a perturbation with dawn-dusk symmetry $\boldsymbol{\xi} = [\mathbf{e}_x\xi_x(x,z) + \mathbf{e}_z\xi_z(x,z)]e^{ik_x x - i\omega t}$, where $(\mathbf{e}_x,\mathbf{e}_y,\mathbf{e}_z)$ are the unit vectors along the (x,y,z) axes, respectively. We call modes of this type as axial tail modes. Here we limit the admissible plasma displacements only to a sub-class of perturbations that have neither y component nor y dependence. Such a constraint leads to the exclusion of the finite-k_y modes such as the high-k_y ideal ballooning instability from the consideration here. Furthermore, since we are interested in the most unstable internal modes, the boundary conditions $\nabla\cdot\boldsymbol{\xi} = 0$ and $\boldsymbol{\xi}_\perp = 0$ are specified. These boundary conditions remove the possibility of ideal interchange instability from considerations here. Of course, the exclusion of the ideal ballooning and interchange instabilities from the sub-class of perturbations considered here does not imply that the 2D tail equilibrium is stable to ideal ballooning or interchange instabilities. Imposing those constraints is a method to isolate the axial tail modes from arbitrary perturbations.

[10] With the above constraints on plasma displacement, the potential energy δW in the static 2D equilibrium for magnetotail can be reduced to

$$\delta W = \frac{1}{2}\int dV\left[|\mathbf{Q}_\perp|^2 + B^2|2\boldsymbol{\kappa}\cdot\boldsymbol{\xi}_\perp + \nabla\cdot\boldsymbol{\xi}_\perp|^2 - 2\left(\boldsymbol{\kappa}\cdot\boldsymbol{\xi}_\perp^*\right)\left(\boldsymbol{\xi}_\perp\cdot\nabla p\right)\right] \quad (3)$$

in the first step of a minimization procedure. For the 2D equilibrium considered here, there is no free energy drive from the current density parallel to equilibrium magnetic field. The only free energy stored in the 2D current sheet is associated with pressure gradient and unfavorable magnetic curvature.

[11] For the 2D equilibrium of the magnetotail, $B_z \sim \epsilon B_x$, where $\epsilon \ll 1$. The variation of equilibrium in the x direction is much slower that the variation in the z direction. To lowest order in $\epsilon = B_z/B_x$, the equilibrium is approximately uniform in the x direction, and the perturbation is approximately wave-like and periodic-like, as represented by $\boldsymbol{\xi} \sim e^{ik_x x - i\omega t}$. The perturbation has also a slow variation in x in response to the slow variation of equilibrium as well as the non-periodic boundary condition in x direction, so the more complete form of perturbation can be approximated by $\boldsymbol{\xi} = [\mathbf{e}_x\xi_x(\epsilon x, z) + \mathbf{e}_z\xi_z(\epsilon x, z)]e^{ik_x x - i\omega t}$. It is the coefficient functions $\xi_x(\epsilon x, z)$ and $\xi_z(\epsilon x, z)$ that are subject to the global boundary conditions in a 2D tail configuration.

[12] The marginal stability condition for the axial mode can be obtained from a further minimization of the δW in (3) through an asymptotic expansion in ε. To lowest order in ε, this procedure leads to an Euler-Lagrangian equation that is a fourth-order linear ordinary equation for ξ_z along z. The solution of the Euler-Lagrangian equation for ξ_z can be used to evaluate the minimized potential energy

$$\delta W = \frac{1}{2}\int dV B_x^2 k_x^2|\xi_z|^2 + \mathcal{O}(\epsilon) \quad (4)$$

The energy principle analysis indicates that for a 2D tail current sheet with $\epsilon = B_z/B_x \ll 1$, any internal perturbation of axial mode type would be stable at leading order in B_z/B_x under the ideal MHD constraint (i.e., "frozen-in-flux" condition). Further MHD analysis of the axial instability of the 2D current sheet with weak normal component B_z requires the consideration of additional dissipative effects such as those associated with resistivity. In order to treat the effects of resistivity and also fully take into account the influence of configuration geometry, we adopt an initial-boundary value approach and linearly evolve an axial initial perturbation of the 2D current sheets using a resistive MHD model implemented in the NIMROD code. The numerical results confirm

the resistive nature of the axial tail instability, which are reported in next section.

3. Resistive MHD Calculations

[13] The resistive MHD model we use for our numerical calculations is based on the following set of equations:

$$\frac{\partial \rho}{\partial t} + \nabla \cdot (\rho \mathbf{u}) = 0 \tag{5}$$

$$\rho\left(\frac{\partial \mathbf{u}}{\partial t} + \mathbf{u} \cdot \nabla \mathbf{u}\right) = \mathbf{J} \times \mathbf{B} - \nabla p + \mu \nabla \cdot (\rho \mathbf{w}) \tag{6}$$

$$\frac{\partial p}{\partial t} + \mathbf{u} \cdot \nabla p = -\gamma p \nabla \cdot \mathbf{u} + \alpha(\gamma - 1)\eta J^2 \tag{7}$$

$$\frac{\partial \mathbf{B}}{\partial t} = -\nabla \times \mathbf{E} \tag{8}$$

$$\mathbf{E} = -\mathbf{u} \times \mathbf{B} + \eta \mathbf{J} \tag{9}$$

$$\mu_0 \mathbf{J} = \nabla \times \mathbf{B} \tag{10}$$

where ρ is the mass density, $\mathbf{u}$ the plasma flow velocity, p the pressure, $\mathbf{E}$ the electric field, $\mathbf{B}$ the magnetic field, $\mathbf{J}$ the current density, $J = |\mathbf{J}|$, the adiabatic index or specific ratio $\gamma = 5/3$, and $\mathbf{w} = \nabla \mathbf{u} + (\nabla \mathbf{u})^{\mathrm{T}} - \frac{2}{3}\mathbf{I}\nabla \cdot \mathbf{u}$ the rate-of-strain tensor [*Braginskii*, 1965]. The dissipation of the system is assumed to primarily come from the anomalous resistivity η and viscosity μ in a weakly collisional or collisionless plasma in the magnetotail. We introduce a multiplier factor α in equation (7) in order to study the effects of Joule heating by setting its value to be either 1 or 0. The resistive Ohm's law in (9) is a simple way to capture the macroscopic consequence of a variety of turbulent dissipation and kinetic demagnetization processes that decouple plasma and magnetic field line motions and break down the "frozen-in-flux" condition in the collisionless magnetotail plasma. We study the MHD stability of the system as a consequence of the violation of the "frozen-in-flux" condition. Following most resistive MHD stability analyses [e.g., *Furth et al*., 1963; *Biskamp*, 1993], we first start our stability calculations in sections 3.1–3.3 without considering the effects of Joule heating by setting $\alpha = 0$. The resistive heating effects do not directly contribute to the necessary mechanisms for the onset of the instability, as confirmed later in our calculations when α is set to be 1 (section 3.4). In absence of Joule heating (i.e., $\alpha = 0$), the system described in the above equations evolves adiabatically and the total entropy is conserved. When $\eta = 0$ and $\mu = 0$, the above equations recover the ideal MHD model used in the energy principle analysis in previous section. Both ideal and resistive MHD models are implemented in the NIMROD code. For the linear calculations carried out in this study, the linearized versions of the equations in (5) to (10) are solved.

[14] The NIMROD code numerically solves the MHD equations in (5) to (10) as an initial-boundary value problem [*Sovinec et al*., 2004]. High-order finite elements are used to represent the two-dimensional x-z plane with arbitrarily shaped boundaries. The third periodic direction in y is discretized using a pseudo-spectral method. In the temporal domain, the solutions are advanced with semi-implicit schemes. For linear modes studied in this work, the dimension in y is represented by a wavenumber $k_y = 0$. In these linear calculations, the initial perturbation first evolves through a transient phase and then settles into an eigenmode of the system when the perturbation starts to grow exponentially at a constant rate and spatial pattern.

[15] A generalized Harris sheet configuration is considered to examine the nature of the axial tail instability as identified from the OpenGGCM simulation of a THEMIS (Time History of Events and Macroscale Interactions During Substorms) substorm event [*Siscoe et al*., 2009; *Zhu et al*., 2009; *Raeder et al*., 2010]. The flux function for a 2D configuration $\Psi = -\lambda \ln \frac{\cosh\left[F(x)\frac{z}{\lambda}\right]}{F(x)}$ can be used to construct an asymptotic equilibrium of a thin current sheet in the near-Earth magnetotail through $\mathbf{B} = \mathbf{e}_y \times \nabla\Psi$ [*Schindler*, 1972]. The corresponding number density is given by $n = n_\infty + \frac{F^2(x)}{2}\left\{\cosh\left[F(x)\frac{z}{\lambda}\right]\right\}^{-2}$, with temperature $T = T_\infty = T(z \to \pm\infty)$ and pressure $p = nT$. A particular 2D current sheet configuration can be specified by a choice of $F(x)$. When $F(x) = 1$, the Harris sheet configuration is recovered, and the parameter λ determines the scale of the current sheet width. Two nontrivial choices of $F(x)$ yield a generalized Harris sheet with a minimum B_z region and another with a uniform B_z within the equatorial plane ($z = 0$), respectively (Figure 1). These two 2D current sheet configurations are employed in our calculations of the axial tail instability. Ideal MHD calculations using the NIMROD code find that the 2D axial tail mode is stable in the one-dimensional (1D) Harris sheet and the 2D generalized Harris sheets. This is consistent with the conclusion from the ideal MHD energy principle analysis in the previous section. In resistive MHD model, our calculations indicate that the axial tail instability can develop in the 2D generalized Harris sheet configurations.

3.1. Harris Sheet ($B_z = 0$)

[16] Before getting into details of the linear calculations of the axial tail instability in generalized Harris sheet configurations, we briefly review the linear properties of resistive tearing instability in a 1D Harris sheet obtained from NIMROD calculations. The Harris sheet configuration is a 1D equilibrium that is often used to model the thin current sheet in middle magnetotail [*Harris*, 1962]. The configuration is defined by an anti-parallel magnetic field $B_x = -\tanh\frac{z}{\lambda}$ and $B_z = 0$, with a neutral sheet located at $z = 0$.

[17] A magnetic field perturbation is initially placed at the center of the computation domain and subsequently advanced in time as an initial-value problem using a linearized version of the full set of resistive MHD equations in equations (5)–(10). A uniform, constant resistivity η and viscosity μ are prescribed. All fields are periodic in the x direction along the current sheet, and the current sheet length in the x direction is chosen as the mode wavelength. The boundary in the z direction of the simulation domain is assumed to be a solid, no-slip wall, so that any potential influence from an external drive or in-flow to the internal process can be excluded. The linear growth rate scales inversely with the Lundquist number S to a fractional power, in agreement with traditional resistive tearing mode theory [*Furth et al*., 1963]. For a Harris sheet with $\lambda = 1$, $S = 10^3$, and the magnetic Prandtl number $Pr_m = 1$, the e-folding time

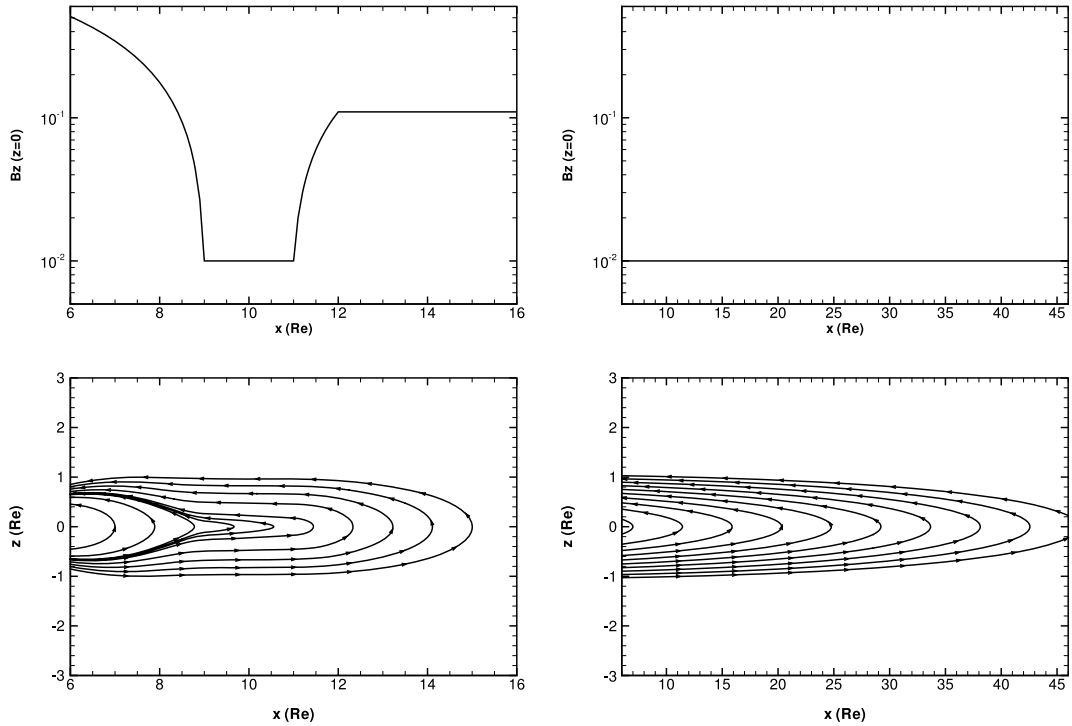

Figure 1. Generalized Harris sheet configurations with a minimum B_z region (Left column) and a uniform B_z (Right column) in the equatorial plane ($z=0$). Top row: B_z profiles along $z=0$ line; Bottom row: Equilibrium magnetic field lines of the configurations.

for the tearing mode growth is about $300\tau_A$, where τ_A is the Alfvénic time measured near the $z=\pm\infty$ boundary of the current sheet. The mode structures of the linear tearing instability show the familiar pattern of a linear, spontaneous, resistive MHD reconnection process (Figure 2, left column). Here and in rest of the paper, all numerical results are presented in normalized, dimensionless units, unless otherwise specified.

3.2. Generalized Harris Sheet with a B_z Minimum Region

[18] In order to model the near-tail configuration around the beginning of the initial growing MHD force imbalance observed in the OpenGGCM simulation of the substorm growth phase, we choose a profile for $F(x)$ so that the normal component of magnetic field B_z in equatorial plane $z=0$ has a minimum region around $10R_E$. This produces an embedded thin 2D current sheet configuration (Figure 1, left column). A similar choice of function *F(x)* was previously used in other simulation studies of tail configurations [e.g., *Pritchett and Büchner*, 1995; *Pritchett and Coroniti*, 1995].

[19] Similar to the Harris sheet case, a perturbation of magnetic field is placed initially around the B_z minimum region, which is time advanced in the NIMROD code using a resistive MHD model. A uniform, constant resistivity η and viscosity μ are used. The boundary of the simulation domain, in both the x and z directions are assumed to be a solid, no-slip wall in order to focus on the internal processes. Such a boundary condition is essentially a field-line-tying boundary condition, which is in general more stable than the incompressible boundary condition considered in the energy principle analysis in section 2. Thus, if the system is stable to perturbations with the incompressible boundary condition, it should also be stable to perturbations that are subject to the line-tying boundary condition in the absence of resistivity and dissipation. On the other hand, in our numerical calculation here, the more stable (hence restrictive) line-tying boundary condition is imposed. If the system becomes unstable to perturbations with the line-tying boundary condition, it is more likely to be unstable to perturbations with the less stable incompressible boundary condition.

[20] A growing eigenmode is obtained from the initial-value calculation only when both the B_z minimum in the equatorial plane and the Lundquist number S are sufficiently small. For a specific case where the minimum value $B_z^{\min} = 0.01$, the current sheet width $\lambda=1$, the Lundquist number $S=10^3$, and the magnetic Prandtl number $Pr_m=1$, the e-folding time of the growing eigenmode is about $1200\tau_A$, where τ_A is the local Alfvénic time near magnetotail lobe locations ($z\rightarrow\pm\infty$). The spatial structures of the linear axial instability show features of both tearing and pressure-driven processes (Figure 2, middle column). Whereas the patterns of perturbed magnetic fields still resemble those of a linear resistive tearing mode in a 1D Harris sheet as shown in the middle column of Figure 2, the spatial distribution of perturbed velocity becomes highly asymmetric in the x direction. In the equatorial plane, the flow from the mode is dominantly in the tailward direction within the minimum B_z region, and the tailward flow is mostly aligned to the dipole-like equilibrium magnetic field Earthward of the minimum B_z region ($x<9$).

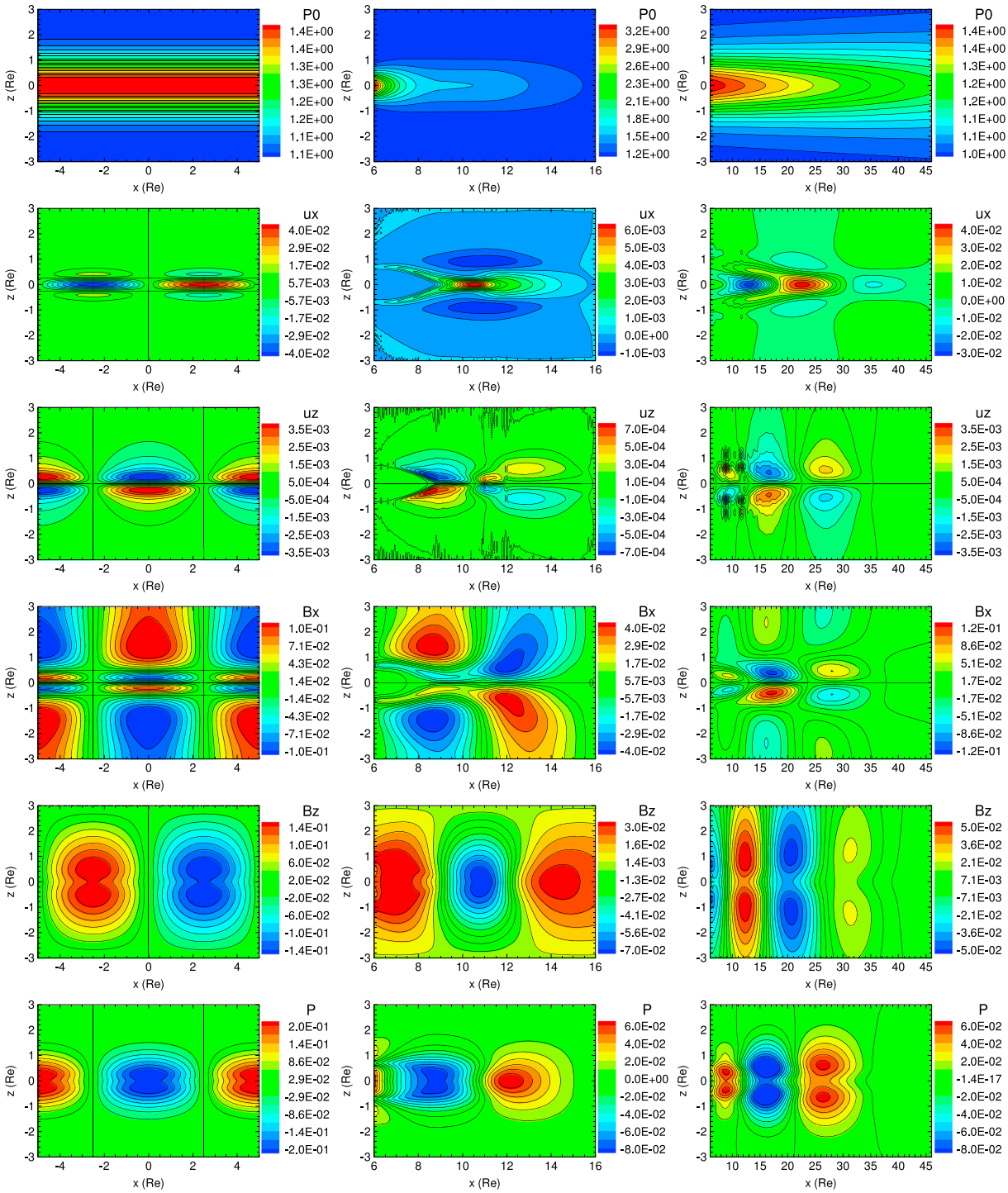

Figure 2. Contours of equilibrium pressure (row 1); tailward flow u_x (row 2); northward flow u_z (row 3); perturbed B_x (row 4); perturbed B_z (row 5); perturbed pressure (row 6) from linear resistive instabilities of 1D Harris sheet (left column); generalized Harris sheets with a minimum B_z region (middle column) and a uniform B_z (right column) along $z=0$ lines, respectively.

Such a dominant tailward flow generates a bubble-blob pair in the pressure that tends to flatten the local pressure profile centered around the region with minimum B_z and thin current sheet. Since the equilibrium pressure gradient near the equatorial plane is mostly Earthward, which is in the same direction of the magnetic field line curvature, such an interchange of pressure directly releases the free internal energy stored in the inhomogeneous distribution of pressure. Thus, in the linear stage of the axial tail instability, the major free energy conversion process is not reconnection but rather a slippage process that is driven by the free energy associated with pressure gradient and made possible through the

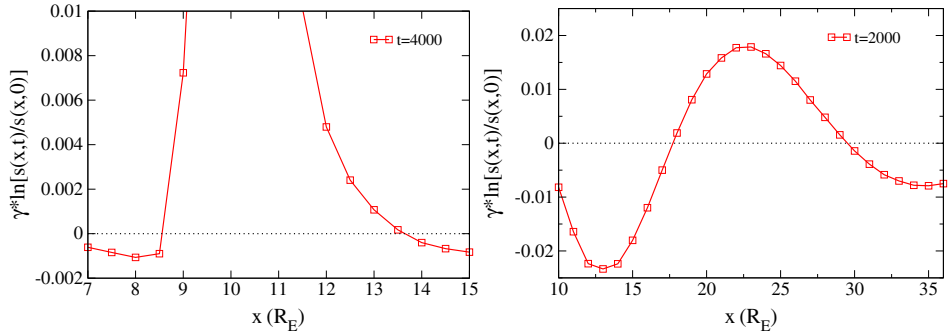

Figure 3. Profiles of entropy perturbation as measured by $\gamma \ln[s(x,t)/s(x,0)]$ along x in the equatorial planes of generalized Harris sheets with minimum B_z region (Left panel), at time $t = 4000$ (red solid line), and with uniform B_z (right panel) along $z = 0$ lines, at time $t = 2000$ (red solid line). The time unit is Alfvénic time. The black dotted line represents the zero axis. The coordinate x is for each fixed location in the equatorial plane where the entropy parameter $s(x,t)$ is calculated.

dissipation due to a finite resistivity. Such a slippage process should not be confused with the ideal interchange instability. The slippage process involves only local and nonuniform displacement of a field line, whereas the ideal interchange process involves global and uniform displacement along a field line. The slippage or resistive pressure-driven process is also a 2D process that only requires plasma displacement within the x-z plane with $k_y = 0$. By contrast, the most unstable ideal interchange instability is essentially a 3D process that is characterized by $k_y \gg 0$.

[21] The perturbed magnetic field associated with the slippage process also tends to reduce B_z as the Earthward pressure gradient becomes smaller. Previously, a current sheet thinning process was demonstrated in simulations as a consequence of the evolution of bubble-blob pairs in entropy distribution [*Yang et al.*, 2011; *Hu et al.*, 2011]. Here our calculation indicates that the formation of such a bubble or blob structure in entropy is the outcome from a self-consistent, spontaneous, internal eigenmode, the axial tail instability. Because the linear axial tail instability does not involve magnetic reconnection, the bubble-blob formation due to the linear axial tail instability does not require topological change of magnetic field lines.

[22] To demonstrate the formation of entropy bubble-blob in our calculations, we measure the evolving global specific entropy $s(x,t) = \int p^{1/\gamma} dl/B$ and entropy parameter $[s(x,t)]^{\gamma}$ [*Wolf et al.*, 2009] at each given time t and each fixed location $(x, z = 0)$ along the equatorial plane from the NIMROD computation results using values of the total pressure and total magnetic fields including both equilibrium and perturbation. Here l is the distance along a field line, which extends between footpoints of each flux tube at the domain boundary. In general, the entropy bubble-blob pair is a 2D spatial structure in entropy distribution within the equatorial plane ($z = 0$) [*Yang et al.*, 2011; *Hu et al.*, 2011]. For the entropy bubble-blob pair formed through the axial tail instability, the structure has only spatial variation in the x direction. In this case, due to a strong B_z field Earthward of the minimum B_z region, the axial tail instability produces a dominantly tailward flow. As a result, the spatial profile of the perturbed entropy parameter along the x axis ($z = 0$) shows a dominant blob structure where $s(x,t) > s(x,0)$ (Figure 3, left panel). A small bubble region where $s(x,t) < s(x,0)$ develops Earthward of the blob region at the same time. The particular pattern of bubble and blob structures depends on the B_z profiles along the equatorial plane of the current sheet.

3.3. Generalized Harris Sheet with a Constant B_z in Equatorial Plane

[23] The slippage nature of the axial tail instability can be further inferred from a linear calculation of the resistive instability of a generalized Harris sheet with a constant B_z in equatorial plane. Such a configuration can be obtained by a choice of $F(x) = e^{-B_n x/\lambda}$, where B_n is a constant value and $B_z|_{z=0} = B_n$. This type of 2D current sheet configuration is well known to be stable to the ion tearing mode in a certain range of parameter space for collisionless plasma [e.g., *Lembége and Pellat*, 1982], but the nature of this resistive MHD instability is the primary concern in this study. To compare with previous cases, we choose a configuration with $B_n = 0.01$ and $\lambda = 1$ (Figure 1, right column).

[24] An initial magnetic perturbation is placed near the center of the computation domain. Under the same boundary conditions as in the previous 2D current sheet case, the initial magnetic perturbation is evolved into a linear resistive instability for a plasma with uniform $S = 10^3$ and $Pr_m = 1$. Due to an overall lower value of the normal component (B_z) in the equatorial plane, the growth rate is larger than the previous current sheet case, which results in an e-folding time about $200\tau_A$, where the Alfvénic time τ_A is similarly defined at lobe locations. The spatial structure of the mode has features of both tearing and pressure-driven processes (Figure 2, right column). The nature of the mode, however, may be further revealed by noting that the center of the mode is not localized at the center of domain along the x axis, even though the normal component of equilibrium magnetic field is constant along $z = 0$ and the initial perturbation is localized tailward of the final mode center location in x. Previous theories on resistive tearing instability of 2D current sheet with finite B_z do not take into account the slow variation of either equilibrium or the global mode structure in x direction and therefore cannot explain the preferred location of

the global mode in x as shown in our numerical results (Figure 2, right column). It is noted that although B_z is constant along the $z=0$ line, the pressure gradient and hence interchange drive decays exponentially tailward. However, the line-bending force is most stabilizing near the Earthward boundary. The final mode location along x can therefore be explained as a balance between the interchange drive and the line-bending stabilization. All the numerical calculations here only include axial mode type of perturbations with $k_y=0$. Since there is no involvement of finite-k_y ideal ballooning instabilities in the calculation, the localization of the global mode structure in these calculation results cannot be explained by ideal ballooning mode theory.

[25] Similarly, a bubble-blob structure forms in the spatial profile of the perturbed entropy parameter as part of the axial tail instability process. In comparison to the case of a current sheet with a minimum B_z region, the bubble-blob structure is more symmetric in the x direction in terms of the magnitude in s (Figure 3, right panel). In both cases, the entropy bubble-blob structures are related to but can be quite different in spatial profile from the bubble-blob structures in pressure.

3.4. Effects of Joule Heating

[26] In previous calculations (sections 3.1), the effects of Joule heating were not included. Traditionally, Joule heating effects are not generally considered essential in dynamics of tearing mode or resistive interchange instabilities [*Furth et al*., 1963; *Biskamp*, 1993]. To address the impact of resistive heating on the axial tail instability, we set $\alpha=1$ in equation (7) and repeat the linear calculations in previous sections.

[27] For all three current sheet configurations, the inclusion of Joule heating does not change the spatial structures of the tearing instability (in Harris sheet) and the axial tail instabilities (in the generalized Harris sheets) qualitatively. For example, the contour structures of the perturbed fields from the axial tail instability of the generalized Harris sheet with a minimum B_z region along the $z=0$ line are essentially the same in the case where the Joule heating is absent and in the case where the Joule heating is included, respectively (Figure 4). In all the current sheet configurations, the Joule heating term essentially does not affect the linear growth rates. For example, for the generalized Harris sheet with a B_z minimum region in equatorial plane, Joule heating effects are able to change the linear growth rate of axial tail instability by less than 1%.

[28] For the linear axial tail instabilities in both general Harris sheet configurations, our calculations indicate that Joule heating does not appear to qualitatively affect the formation of the bubble-blob structure in entropy distribution (Figure 5). With the inclusion of Joule heating effects, the profiles of entropy perturbation as measured by $\gamma\ln[s(x,t)/s(x,0)]$ along x in the equatorial planes of generalized Harris sheets for the case with minimum B_z region at time $t=4000$ and for the case with uniform B_z along $z=0$ line at time $t=2000$ show similar bubble-blob structures as those in previous calculations where the Joule heating effects are absent (Figures 3 and 5). These calculation results suggest that the formation of the bubble-blob structure is primarily a redistribution in entropy as a consequence of the linear axial tail instability. In comparison, the contribution from Joule heating effects does not qualitatively or significantly change the formation of bubble-blob pattern.

4. Summary and Discussion

[29] In summary, our ideal MHD energy principle analysis indicates that a 2D tail configuration is stable to the axial tail mode with $k_y=0$ to lowest order in B_z/B_x with the ideal MHD constraint (i.e., the "frozen-in-flux" condition). Calculations using a resistive model implemented in the NIMROD code find linear axial tail instability on closed field lines in the 2D generalized Harris sheets. The axial tail mode is unstable in low S regime and small B_z regions. Such a resistive axial tail instability would by many researchers be considered as tearing instability in a two-dimensional tail configuration. Unlike the resistive tearing mode in the 1D Harris sheet, the linear development of this axial tail instability does not involve any reconnection process. Rather, the nature of the axial tail mode is dominantly a slippage process between neighboring flux tubes carrying different pressure or entropy values as facilitated by resistivity. Such a slippage process is local along the field line, driven by the interchange free energy, and non-ideal due to the involvement of resistivity. The axial mode of the 2D generalized Harris sheet obtained in NIMROD simulations can be used to explain the growth and structure of the axial mode associated with the initial growing MHD force imbalance found in OpenGGCM simulations. A natural product of this axial instability process is the formation of the bubble-blob pairs in pressure and entropy distribution. Note that the effects of Joule heating do not seem to significantly change the formation of bubble-blob pattern in entropy. This suggests that as a consequence of the linear axial tail instability, the formation of bubble-blob structure is primarily a redistribution in entropy.

[30] As suggested by recent global resistive MHD simulations of substorm events, these axial modes can be a major cause of the initial growing MHD force imbalance and, in the nonlinear stage, lead to the subsequent formation of a near-Earth neutral line and initiate a reconnection process prior to a substorm onset. A natural consequence of the axial tail instability is the facilitation of a configuration that ultimately produces reconnection. The time scale of the axial tail instability generally resembles the time scale of the substorm growth phase rather than the rapid time scale of an expansion onset. However, detailed quantitative calculations depend on the parameter regimes and equilibrium configurations. The role of the linear axial tail instability appears to be setting up a favorable condition for the formation of an X-line and initiating the subsequent reconnection. Whereas the linear axial tail instability may correspond to the slower time scale of the substorm growth phase, it is the ensuing fast reconnection process that may account for the rapid time scale of a substorm expansion onset. Such a scenario appears to be consistent with the results from previous global MHD simulations of a substorm event [*Raeder et al*., 2010].

[31] We use the term "axial tail instability" to emphasize the non-reconnecting nature of the process identified in our work. Such a process has been studied in many previous works where it was often referred to as a "resistive tearing mode" of 2D current sheet with finite B_z [e.g., *Schindler*, 1974; *Galeev and Zelenyi*, 1976; *Birn et al*., 1975; *Birn*,

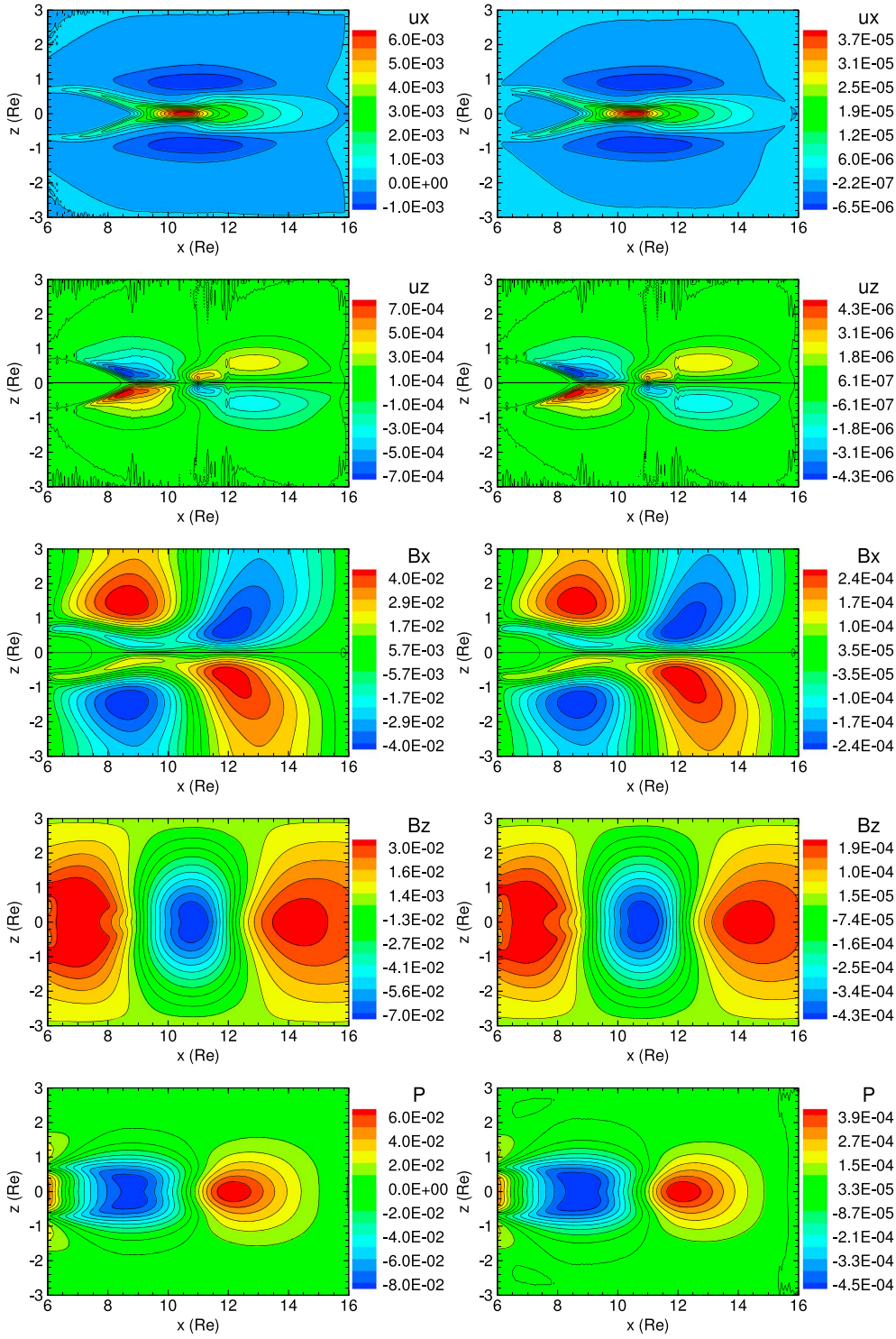

Figure 4. Contours of tailward flow u_x (row 1); northward flow u_z (row 2); perturbed B_x (row 3); perturbed B_z (row 4); perturbed pressure (row 5) from the axial tail instability of the generalized Harris sheet with a minimum B_z region along $z=0$ line in absence (left column) and in presence (right column) of Joule heating, respectively.

1980; *Janicke*, 1980; *Hesse and Birn*, 1994; *Harrold et al*., 1995; *Sundaram and Fairfield*, 1997; *Sitnov et al*., 2002]. Most previous eigenvalue-based analytical and numerical analyses on the resistive instability of the 2D magnetotail configuration did not take into account the non-periodic variation of either the equilibrium or the global mode structure along the x direction [*Galeev and Zelenyi*, 1976; *Janicke*, 1980; *Harrold et al*., 1995; *Sundaram and Fairfield*, 1997]. Other previous initial-value-based numerical analyses considered the non-periodic variation of the equilibrium and

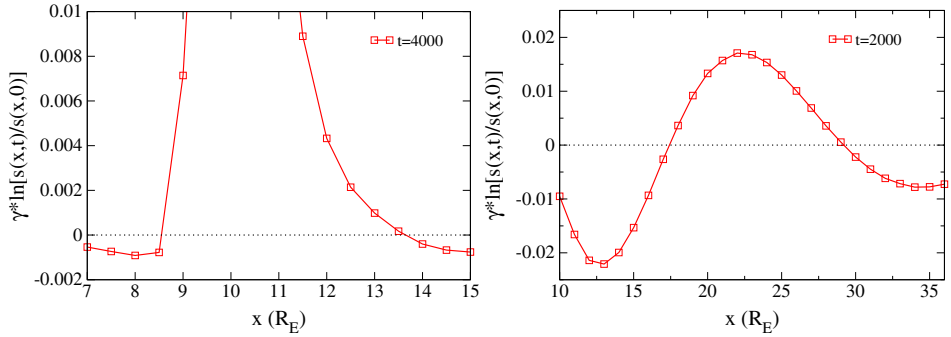

Figure 5. Profiles of entropy perturbation from calculations where the Joule heating term in equation (7) is included. The entropy perturbation is measured by $\gamma \ln[s(x,t)/s(x,0)]$ as a function of x in the equatorial planes of generalized Harris sheets with minimum B_z region (Left panel), at time $t = 4000$ (red solid line), and with uniform B_z (right panel) along $z = 0$ lines, at time $t = 2000$ (red solid line). The time unit is Alfvénic time. The black dotted line represents the zero axis. The coordinate x is for each fixed location in the equatorial plane where the entropy parameter $s(x,t)$ is calculated.

the global mode structure along the x direction [*Birn*, 1980; *Hesse and Birn*, 1994]. One major difference between our work and the previous studies on the resistive instability of the 2D magnetotail configuration lies in the interpretation of the nature of the instability. The nature of this axial tail instability is a relaxation process through the slippage of neighboring flux tubes with different pressure values. Such a slippage process is made possible in the MHD model by the inclusion of resistivity. In reality, this mechanism could derive from other non-ideal terms in Ohm's law. This is a fundamentally different mechanism from the linear tearing instability of a 1D Harris sheet.

[32] The linear axial tail instability does not involve magnetic reconnection due to the presence of nonzero B_z and preserved magnetic field line topology. In contrast, the resistive tearing instability in a 1D current sheet involves magnetic reconnection and the change of magnetic field line topology right from the beginning of the process. One fundamental question in substorm physics is whether the initial trigger process involves a magnetic reconnection or not. Answer to this question would determine where and when the initial trigger for substorm onset occurs. In addition, whether an instability involves a magnetic reconnection reveals the nature of the relaxation process. The resistive tearing instability is a process that converts free magnetic energy to kinetic energy through the change of field line topology. On the other hand, the axial tail instability mainly converts the free internal energy to kinetic energy through the slippage of neighboring flux tubes with different pressure values.

[33] The axial tail mode is significantly more stable than the resistive tearing mode in a 1D current sheet due to the presence of finite B_z that characterizes a 2D current sheet. Under the same conditions as in a 1D current sheet, only when B_z is below a certain critical value would the axial tail mode become unstable. This is a direct consequence of the preservation of magnetic field topology due to the lack of magnetic reconnection process in the axial tail mode [e.g., *Harrold et al.*, 1995].

[34] The growth rate scaling of the axial tail instability with resistivity is different from the resistive tearing mode of a 1D current sheet in general. In particular, the growth rate scaling of the axial tail instability with resistivity depends on the relative strength of the background normal magnetic component B_z (as normalized with the lobe magnetic field). Earlier work by *Janicke* [1980] considered the 2D current sheet regime where the B_z is extremely small (i.e., $B_z \to 0$), so that the growth rate scaling with resistivity, as well as the mode pattern is similar to the resistive tearing instability of a 1D current sheet. On the other hand, *Harrold et al.* [1995] considered another regime of the 2D current sheet where B_z is sufficiently larger, so that the growth rate scaling is close to that of a magnetic diffusion. In general, the growth rate scaling of the axial tail instability is more complicated than the two extreme regimes.

[35] The spatial structure of the axial tail instability depends on the equilibrium pressure and B_z profiles in the x direction, and the center of the mode structure has a preferred location in the x direction independent of the initial condition. In contrast, the mode structure of the resistive tearing instability would prefer the neutral sheet location where $B_z = 0$. In the 1D current sheet, the neutral sheet is the entire $z = 0$ line and the equilibrium is invariant along the x direction. Thus, there is not a preferred location for the center of the resistive tearing mode along $z = 0$, which is purely determined by the initial and boundary conditions.

[36] One consequence of the axial tail instability is the formation of entropy bubble-blob pair, which in nonlinear stage, as shown in previous work [*Yang et al.*, 2011; *Hu et al.*, 2011], can accelerate current sheet thinning, formation of X-line, and eventually reconnection. One main take-away message from these findings is that even though reconnection process often precedes a substorm onset expansion, the onset trigger process may not start from reconnection out of a 2D current sheet equilibrium. The reconnection process itself can be initiated by the axial tail instability, which is a non-reconnecting, flux-tube slippage process on close field lines with finite B_z in the near-Earth magnetotail.

[37] So far, we have shown in this work that bubble-blob pairs can form from the axial tail instability in the 2D MHD simulation and this instability may help explain the bubble-blob pairs found in observation and other simulations. This does not necessarily imply that any bubble-blob pair found in observations or other simulations is a natural consequence

of the axial tail instability alone. Indeed, 3D processes such as the interchange and ballooning instabilities, as well as their couplings to the axial tail instability, may introduce complications to the bubble-blob formation process. In addition, the resistive MHD model may not provide an accurate model for the near-Earth magnetotail dynamics. Many other non-ideal effects, such as the two-fluid and kinetic physics, can potentially influence or enhance the grow rate of the linear axial tail instability. Examination of those possibilities are subjects of future work. The main purpose of this work is to propose a new scenario for understanding the nature of the initial growing MHD force imbalance that is crucial in triggering the reconnection itself in the near-Earth magnetotail.

[38] **Acknowledgments.** This research was supported by NSF grants AGS-0902360 and PHY-0821899. Work at UNH was supported by NASA grant NAS5-02099 (THEMIS). P. Zhu is grateful for discussions with A. Bhattacharjee, J. Birn, M. Sitnov, F. Toffoletto, R. Wolf, and J. Yang. The computational work used the NSF TeraGrid resources provided by TACC under grant number TG-ATM070010 and the resources of NERSC, which is supported by DOE under Contract No. DE-AC02-05CH11231.

References

Bernstein, I. B., E. A. Frieman, M. D. Kruskal, and R. M. Kulsrud (1958), An energy principle for hydromagnetic stability problems, *Proc. R. Soc. London*, *244*, 17–40.

Birn, J. (1980), Computer studies of the dynamic evolution of the geomagnetic tail, *J. Geophys. Res.*, *85*, 1214–1222.

Birn, J., R. Sommer, and K. Schindler (1975), Open and closed magnetospheric tail configurations and their stability, *Astrophys. Space Sci.*, *35*, 389.

Biskamp, D. (1993), Nonlinear Magnetohydrodynamics, Cambridge University Press, Cambridge, UK.

Borovsky, J. E., and H. O. Funsten (2003), MHD turbulence in the Earth's plasma sheet: Dynamics, dissipation, and driving, *J. Geophys. Res.*, *108*(A7), 1284, doi:10.1029/2002JA009625.

Braginskii, S. I. (1965), *Reviews of Plasma Physics*, vol. 1, p. 205, edited by M. A. Leontovich, Consultants Bureau, New York.

Brittnacher, M., K. B. Quest, and H. Karimabadi (1994), On the energy principle and ion tearing in the magnetotail, *Geophys. Res. Lett.*, *21*(15), 1591–1594, doi:10.1029/94GL01697.

Cattell, C. A. (1996), Experimental evaluation of the Lundquist number for the Earth's magnetopause and magnetotail, *J. Geophys. Res.*, *101*, 27,309.

Furth, H. P., J. Killeen, and M. N. Rosenbluth (1963), Finite resistivity instabilities of a sheet pinch, *Phys. Fluids*, *6*, 459, doi:10.1063/1.1706761.

Galeev, A. A., and L. M. Zelenyi (1976), Tearing instability in plasma configurations, *Sov. Phys. JETP*, *43*, 1113.

Harris, E. G. (1962), On a plasma sheath separating regions of oppositely directed magnetic field, *Nuovo Cimento*, *23*, 115.

Harrold, B. G., A. Bhattacharjee, and X. G. Wang (1995), Tearing stability of the two-dimensional magnetotail, *Phys. Plasmas*, *2*, 3857–3864.

Hesse, M., and J. Birn (1994), MHD modeling of magnetotail instability for localized resistivity, *J. Geophys. Res.*, *99*, 8565–8576.

Hu, B., R. A. Wolf, F. R. Toffoletto, J. Yang, and J. Raeder (2011), Consequences of violation of frozen-in-flux: Evidence from OpenGGCM simulations, *J. Geophys. Res.*, *116*, A06223, doi:10.1029/2011JA016667.

Janicke, L. (1980), Resistive tearing mode in weakly two-dimensional neutral sheets. *Phys. Fluids*, *23*, 1843–1849.

Lembége, B., and R. Pellat (1982), Stability of a thick two-dimensional quasineutral sheet, *Phys. Fluids*, *25*, 1995.

Miura, A. (2007), A magnetospheric energy principle for hydromagnetic stability problems, *J. Geophys. Res.*, *112*, A06234, doi:10.1029/2006JA011992.

Pellat, R., F. V. Coroniti, and P. L. Pritchett (1991), Does ion tearing exist?, *Geophys. Res. Lett.*, *18*(2), 143–146, doi:10.1029/91GL00123.

Pritchett, P. L. (1994), Effect of electron dynamicson collisionless reconnection in two-dimensional magnetotail equilibria, *J. Geophys. Res.*, *99*(A4), 5935–594.

Pritchett, P. L., and J. Büchner (1995), Collisionless reconnection in configurations with a minimum in the equatorial magnetic field and with magnetic shear, *J. Geophys. Res.*, *100*, 3601.

Pritchett, P. L., and F. V. Coroniti (1995), Formation of thin current sheets during plasma sheet convection, *J. Geophys. Res.*, *100*, 23,551–23,566.

Quest, K., H. Karimabadi, and M. Brittnacher (1996), Consequences of particle conservation along a flux surface for magnetotail tearing, *J. Geophys. Res.*, *101*(A1), 179–183, doi:10.1029/95JA02986.

Raeder, J., D. Larson, W. Li, L. Kepko, and T. Fuller-Rowell (2008), OpenGGCM simulations for the THEMIS mission, *Space Sci. Rev.*, *141*, 535–555, doi:10.1007/s11214-008-9421-5.

Raeder, J., P. Zhu, Y. Ge, and G. Siscoe (2010), Open Geospace General Circulation Model simulation of a substorm: Axial tail instability and ballooning mode preceding substorm onset, *J. Geophys. Res.*, *115*, A00I16, doi:10.1029/2010JA015876.

Schindler, K. (1972), A self-consistent theory of the tail of the magnetosphere, in *Earth's Magnetospheric Processes*, edited by B. M. McCormac, p. 200, D. Reidel, Norwell, Mass.

Schindler, K. (1974), A theory of the substorm mechanism, *J. Geophys. Res.*, *79*, 2803–2810.

Siscoe, G. L., M. M. Kuznetsova, and J. Raeder (2009), Search for an onset mechanism that operates for both CMEs and substorms, *Ann. Geophys.*, *27*, 3141–3146.

Sitnov, M. I., and M. M. Swisdak (2011), Formation of dipolarization fronts as a part of the magnetic reconnection onset process in two-dimensional current sheets, abstract SM13C-2093 presented at 2011 Fall Meeting, AGU, San Francisco, Calif., 5–9 Dec.

Sitnov, M. I., A. S. Sharma, P. N. Guzdar, and P. H. Yoon (2002), Reconnection onset in the tail of Earth's magnetosphere, *J. Geophys. Res.*, *107*, 1256.

Sovinec, C., et al. (2004), Nonlinear magnetohydrodynamics with high-order finite elements, *J. Comput. Phys.*, *195*, 355.

Sundaram, A. K., and D. H. Fairfield (1997), Stability of resistive MHD tearing and ballooning modes in the tail current sheet, *J. Geophys. Res.*, *102*, 19,913–19,926, doi:10.1029/97JA01241.

Weygand, J. M., et al. (2005), Plasma sheet turbulence observed by Cluster II, *J. Geophys. Res.*, *110*, A01,205, doi:10.1029/2004JA010581.

Wolf, R. A., Y. Wan, X. Xing, J.-C. Zhang, and S. Sazykin (2009), Entropy and plasma sheet transport, *J. Geophys. Res.*, *114*, A00D05, doi:10.1029/2009JA014044.

Yang, J., R. A. Wolf, and F. R. Toffoletto (2011), Accelerated thinning of the near-Earth plasma sheet caused by a bubble-blob pair, *Geophys. Res. Lett.*, *38*, L01107, doi:10.1029/2010GL045993.

Zhu, P., J. Raeder, K. Germaschewski, and C. C. Hegna (2009), Initiation of ballooning instability in the near-Earth plasma sheet prior to the 23 March 2007 THEMIS substorm expansion onset, *Ann. Geophys.*, *27*, 1129–1138.